The impact of mass-dependent stochasticity at cosmic dawn

Viola Gelli,[1,2] Charlotte Mason,[1,2] and Christopher C. Hayward[3]

[1] Cosmic Dawn Center (DAWN)
[2] Niels Bohr Institute, University of Copenhagen, Jagtvej 128, 2200 København N, Denmark
[3] Center for Computational Astrophysics, Flatiron Institute, 162 Fifth Avenue, New York, NY 10010, USA

Abstract

JWST is unveiling a surprising lack of evolution in the number densities of ultraviolet-selected (UV) galaxies at redshift $z \gtrsim 10$. At the same time, observations and simulations are providing evidence for highly bursty star formation in high-z galaxies, resulting in significant scatter in their UV luminosities. Galaxies in low-mass dark matter halos are expected to experience most stochasticity due to their shallow potential wells. Here, we explore the impact of a mass-dependent stochasticity using a simple analytical model. We assume that scatter in the $M_{\rm UV} - M_h$ relation increases towards lower halo masses, following the decrease in halo escape velocity, $\sigma_{\rm UV} \sim M_h^{-1/3}$, independent of redshift. Since low-mass halos are more dominant in the early universe, this model naturally predicts an increase in UV luminosity functions (LFs) at high redshifts compared to models without scatter. We make predictions for additional observables which would be affected by stochasticity and could be used to constrain its amplitude, finding: (i) galaxies are less clustered compared to the no-scatter scenario, with the difference increasing at higher-z; (ii) assuming star-bursting galaxies dominate the ionizing photon budget implies reionization starts earlier and is more gradual compared to the no-scatter case, (iii) at fixed UV magnitude galaxies should exhibit wide ranges of UV slopes, nebular emission line strengths and Balmer breaks. Comparing to observations, the mass-dependent stochasticity model successfully reproduces the observed LFs up to $z \sim 12$. However, the model cannot match the observed $z \sim 14$ LFs, implying additional physical processes enhance star formation efficiency in the earliest galaxies.

Keywords: High-redshift galaxies; Galaxy evolution; Cosmology

1. INTRODUCTION

During its first two years of observations, the James Webb Space Telescope (JWST) has revealed a puzzling abundance of luminous galaxies at high redshifts ($z > 10$) that are challenging our understanding of early star formation. Numerous observations of ultraviolet (UV) bright galaxies have been reported, and the photometrically derived UV luminosity functions (LF) show a surprising lack of evolution, across a range of luminosities, during the first ~ 500 Myr after the Big Bang (e.g. Adams et al. 2023; Atek et al. 2023a; Castellano et al. 2022; Donnan et al. 2024; Finkelstein et al. 2023; Harikane et al. 2023; McLeod et al. 2024; Pérez-González et al. 2023; Bouwens et al. 2023). Most pre-JWST mod-

els struggle to reproduce the observed trends, prompting the emergence of numerous new theories in an effort to solve this discrepancy.

One possibility is a systematic enhancement of the median UV flux of high-z galaxies. This enhancement may be achieved through different mechanisms, such as: higher star formation efficiencies (Mason et al. 2023; Dekel et al. 2023; Inayoshi et al. 2022; Li et al. 2023), top-heavier initial mass functions (although likely not sufficient to reproduce the observations up to the highest z, e.g., Rasmussen Cueto et al. 2023; Trinca et al. 2024), or efficient dust removal (Ferrara 2023; Fiore et al. 2023).

An alternative explanation is the presence of a stochasticity in the galaxies luminosities: the relation between the UV magnitude of a galaxy ($M_{\rm UV}$) and the mass of the dark matter halo in which it resides (M_h) may not be univocal, but rather characterized by a dispersion σ_{UV} (e.g. Mason et al. 2023; Mirocha & Furlanetto 2023; Shen et al. 2023; Kravtsov & Belokurov 2024).

Corresponding author: Viola Gelli
viola.gelli@nbi.ku.dk

In this way, the increased normalization of the LFs can be explained by the up-scattered luminosities in the numerous low-mass halos dominating the high-z population.

A physical mechanism that can naturally produce a scatter in the UV luminosities of galaxies is a bursty star formation history (SFH). The complex interplay between multiple mechanisms, such as internal feedback processes, the continuous inflow of gas from the cosmic web and mergers, can cause a stochastic behavior in the star formation rate (SFR) of high-z galaxies, making their UV luminosity fluctuate over time (e.g. Sparre et al. 2017; Furlanetto & Mirocha 2022; Sun et al. 2023a). Both JWST observations and cosmological simulations suggest that star formation in the first billion years after the Big Bang may have occurred in a particularly bursty fashion.

From the observational side, deep JWST surveys are revealing a broad range of SFRs in high-z star forming galaxies (e.g. Curti et al. 2023; Endsley et al. 2023b). In particular, Endsley et al. (2023b) recently found that UV-faint galaxies ($M_{\rm UV} \gtrsim -17$) often have weaker nebular emission lines and can be experiencing a downturn in star formation compared to UV-bright galaxies ($M_{\rm UV} \lesssim -20$) which are more likely to have strong emission lines and to be in an up-turn of star formation. This is consistent with a picture whereby the bright-end of the UV LF is dominated by galaxies which have been up-scattered, whereas fainter galaxies show a range of star formation history stages. Moreover, the first detections of quenched low-mass galaxies ($M_\star < 10^9 {\rm M}_\odot$) at $z > 5$ (Looser et al. 2023a,b; Strait et al. 2023) can be interpreted as post-starburst galaxies undergoing temporary periods of quiescence due to a highly bursty and feedback-regulated star formation (Gelli et al. 2023, 2024; Dome et al. 2023). The timescales on which these SFR variations occur tightly depend on the ongoing feedback processes within the galaxy (e.g., Iyer et al. 2020). Thus, constraining the level of stochasticity and burstiness of high-z systems is essential for understanding the physical mechanisms driving their evolution.

State-of-the-art cosmological simulations also predict a highly time variable star formation in the early Universe (e.g. Ma et al. 2018; Pallottini et al. 2022). However, whether the stochasticity in the SFRs of early galaxies is sufficient to explain the high number densities observed is still debated: Pallottini & Ferrara (2023) argue that an additional source of luminosity is needed already at $z \sim 8$, while Sun et al. (2023b) finds that $z \sim 8 - 12$ LFs can be reproduced with FIRE-2 simulations, which show strongly time-variable SFHs. Meanwhile, analytical studies have shown that, to match the

observed LFs, the level of scatter in the UV luminosities σ_{UV} needs to increase significantly above $z \gtrsim 10$ (Muñoz et al. 2023; Shen et al. 2023; Mason et al. 2023; Kravtsov & Belokurov 2024). In these works, the UV scatter is assumed to be independent of the halo mass. However, low-mass halos are intrinsically characterized by shallower potential wells and the galaxies residing in them are expected to be more sensitive to all those feedback and environmental processes that drive bursty star formation (e.g. Gelli et al. 2020; Furlanetto & Mirocha 2022; Legrand et al. 2022; Hopkins et al. 2023). For this reason, we expect stochasticity to be more relevant for lower mass halos, which, in a ΛCDM Universe, dominate the galaxy population at progressively higher-z.

In this paper, we develop a simple analytical model to explore a *mass-dependent* UV scatter, i.e. increasing towards lower halo masses, independent of the redshift, described in Section 2. We analyze the impact of this mass-dependent UV scatter on the LF, but also on other key observables: the neutral fraction in the intergalactic medium (IGM), the galaxy bias and spectral features, providing unique independent tools to help us constrain the relevance of bursty star formation in high-z galaxies. These results are presented in Section 3. We discuss our results in the context of the $z > 12$ LFs in Section 4 and present our conclusions in Section 5. We assume a flat ΛCDM cosmology with $\Omega_m = 0.3$, $\Omega_\Lambda = 0.7$ and $h = 0.7$.

2. MODELING THE MASS-DEPENDENT UV SCATTER

We model the stochasticity by assuming a mass-dependent but *redshift-independent* scatter $\sigma_{\rm UV}(M_h)$, describing the dispersion in the $M_{\rm UV} - M_h$ relation, which decreases with halo mass. This is motivated by cosmological simulations such as FIRE-2 which find a decreasing trend with the halo mass, without a significant evolution between $z \sim 8 - 12$ (Sun et al. 2023b). This scatter can be well approximated by a power-law relation $\sigma_{\rm UV}(M_h) = a \log M_h/{\rm M}_\odot + b$. We assume a fiducial model with $a = -0.34$ and $b = 4.5$, shown in the bottom panel of Fig. 1, obtained by fitting the results of the FIRE-2 simulations at $z \sim 8$ (derived from Fig. 1 of Sun et al. 2023b). Interestingly, this scaling with halo mass is very similar to the $M_h^{-1/3}$ scaling expected if the stochasticity scales with the inverse of halos' escape velocities – i.e. more tightly bound halos can retain more gas and have lower stochasticity.

To include the scatter in our modeling, we adopt the conditional luminosity function (CLF) approach, following Ren et al. (2019) (see also Whitler et al. 2020). The
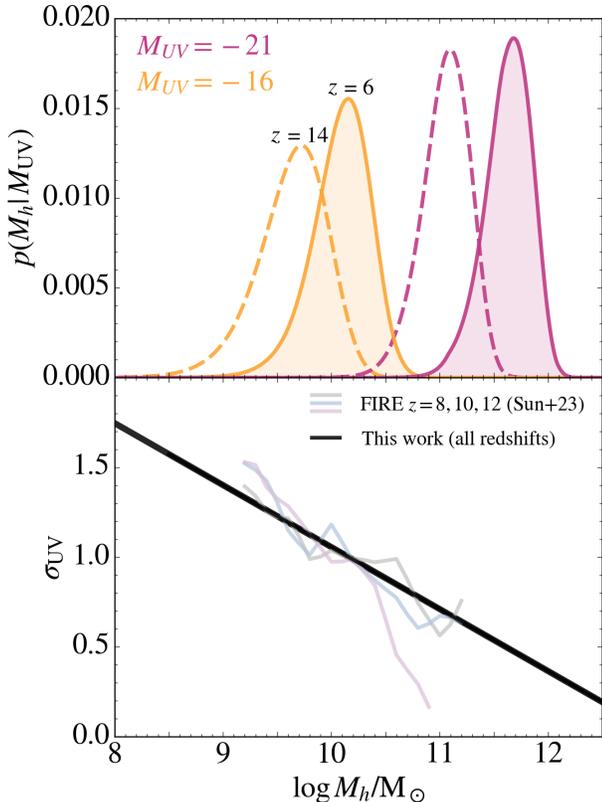
Figure 1. *Top panel:* Probability distribution of halo masses at given UV magnitude M_{UV}, with corresponding scatter σ determined by the model in the bottom panel. The distributions are shown for three different redshifts, highlighting the broadening of the distributions towards earlier epochs. *Bottom panel:* Mass-dependent UV scatter $\sigma_{UV}(M_h)$ as a function of the halo mass M_h. The black line shows the fiducial model used in this work, for all redshifts.

probability of a dark matter halo with mass M_h to host a galaxy with magnitude M_{UV} is given by:

$$
p(M_{UV} \mid M_h) =
\frac{1}{\sqrt{2\pi}\sigma_{UV}(M_h)} \exp\left(\frac{-[M_{UV} - M_{UV,c}(M_h,z)]^2}{2\sigma_{UV}^2(M_h)} \right), \quad (1)
$$

where $M_{UV,c}$ is the median magnitude at a given redshift z and halo mass M_h. We derive it by following Mason et al. (2015, 2023), assuming $\langle \text{SFR} \rangle \propto \epsilon_\star f_b M_h$, where f_b is the cosmic baryon fraction and $\epsilon_\star$ the star formation efficiency, and then using STARBURST99 (Leitherer et al. 1999)[1] to derive M_{UV}. We assume a mass-

dependent star formation efficiency $\epsilon_\star(M_h) \sim M_\star/M_h$, and we calibrate[2] it at a single redshift $z \sim 5$ to reproduce the observed UVLFs by Bouwens et al. (2023) (see also Mason et al. 2015; Ren et al. 2019; Mirocha & Furlanetto 2023). Like the UV scatter, once calibrated, the derived star formation efficiency is assumed to be *redshift independent*.

We can derive halo mass distributions $p(M_h \mid M_{UV})$ using a numerical approach, evaluating the probability in Equation 1 for an array of halo masses at fixed M_{UV} and z (see also Whitler et al. 2020). The results are shown in the top panel of Fig. 1 for two different magnitudes and redshifts. The position of the peak of the distribution is determined by the median $M_{UV,c}(M_h,z)$, while the width of the distribution is determined by the scatter $\sigma_{UV}(M_h)$ and is independent of the redshift. At fixed redshift, brighter galaxies are more likely to be hosted by larger dark matter halos. Note however that here we are not weighting by the halo mass function. As lower mass halos are in reality more numerous, galaxies we observe at fixed UV magnitudes will be more likely to be hosted in lower mass halos, as it will be evident in the next section. The dispersion around the median M_h is larger for lower luminosities. This is a direct consequence of the increasing σ_{UV} towards lower masses, making lower mass halos have high probability to appear with a wider range of luminosities.

Comparing the different redshifts, we can see that there is a broadening of the distribution towards high-z, meaning that galaxies at a given M_{UV} can be hosted at higher z by a broader range of halos with respect to their lower z analogues. This behavior is due to the combined effect of: (i) the increasing median luminosity $M_{UV,c}(M_h,z)$ with the redshift – i.e. at fixed halo mass, galaxies are on-average more luminous at higher redshift, due to higher SFRs, and (ii) the increasing scatter σ_{UV} in lower mass halos.

In the following sections we determine and analyze the expected impact of such mass-dependent UV scatter on different observables (UVLFs, SFR density, neutral hydrogen fractions, spectral features).

3. RESULTS

We present our model for the UV luminosity function in Section 3.1 and the luminosity density in Section 3.2. In Section 3.3 we make predictions for other independent observables: galaxy clustering, the reionization timeline,

---

[1] We use PADOVA stellar tracks (Bertelli et al. 1994) and assume a Kroupa (2001) initial mass function between 0.1 and $100 M_\odot$. However we note that the following results are not sensitive to these specific choices.

[2] We note that when introducing mass-independent scatter, Ren et al. (2019) required a break in $\epsilon_\star(M_h)$ above $M_h \gtrsim 10^{11.5}$ to match the bright-end of the LF, however, this is not necessary in our model as $\sigma_{UV}(M_h)$ is so low at these high halo masses.
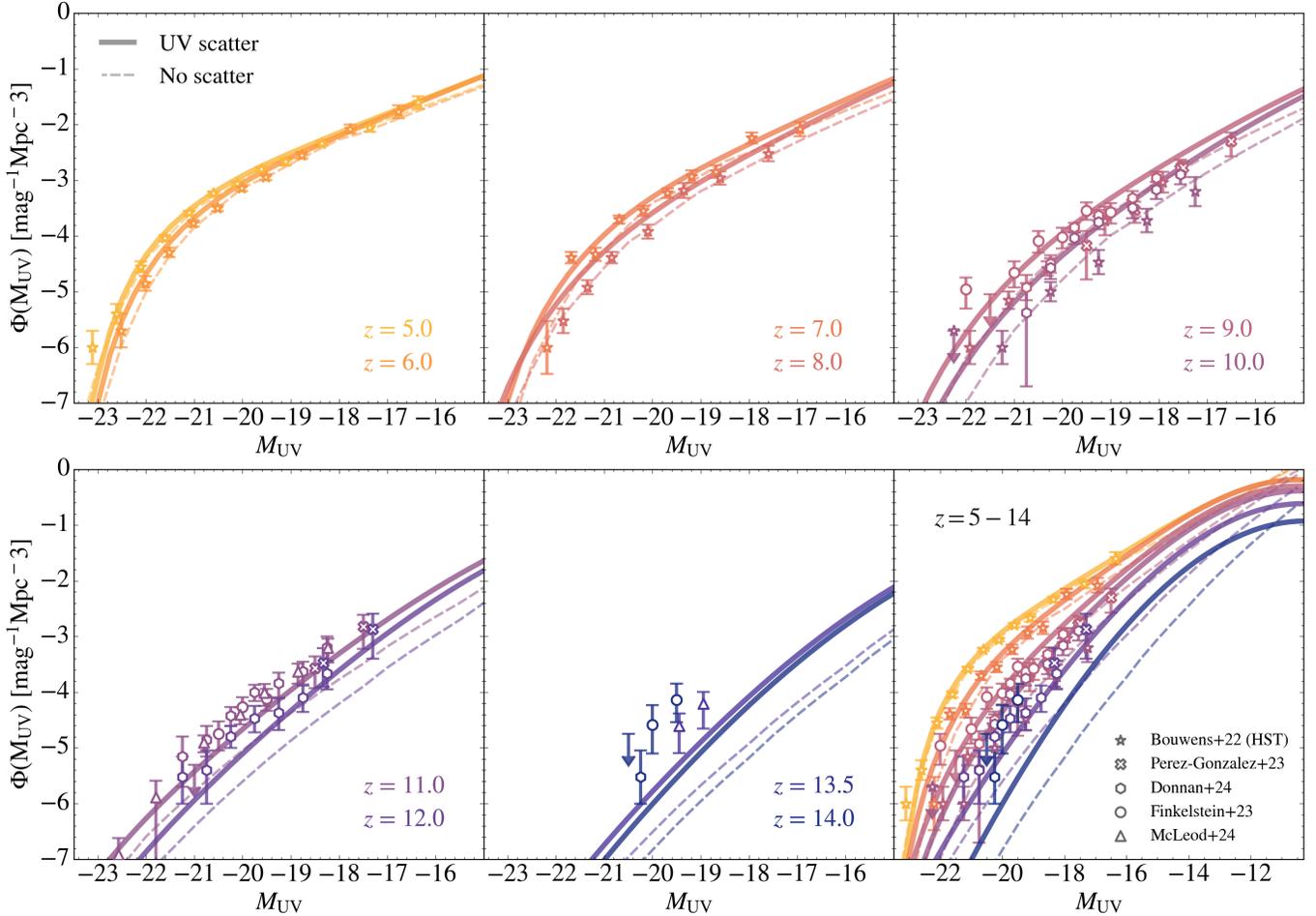
Figure 2. UV LF for the mass-dependent UV scatter model (solid lines) and the no-scatter model (dashed lines) at redshifts from $z = 5$ to 14. Also shown are observations by Bouwens et al. (2022a); Finkelstein et al. (2023); Pérez-González et al. (2023); Donnan et al. (2024); McLeod et al. (2024).

and galaxy SEDs; which could be combined with the LF to constrain the level of stochasticity.

3.1. *Luminosity function*

Following the CLF approach, we derive the luminosity functions by integrating the number density of dark matter halos, weighted by the probability that a halo M_h hosts a galaxy with magnitude M_{UV}:

$$\Phi(M_{UV}) = \int_{M_{h,min}}^{\infty} dM_h \, p(M_{UV} \mid M_h) \frac{dn}{dM_h}; \qquad (2)$$

where $p(M_{UV} \mid M_h)$ is given by Equation 1, and for dn/dM_h we use the halo mass function (HMF) from Reed et al. (2007). We set a lower limit to the integral, $M_{h,min}$, to prevent the unphysical effect of very low-mass halos forming stars with extremely large UV scatter. Its value is set at each redshift as the minimum halo mass for which atomic cooling can occur, i.e. corresponding to a virial temperature of $T_{vir} \sim 10^4$K (e.g. Bromm & Yoshida 2011). Following Mason et al. (2015,

2023) we add dust attenuation using the Meurer et al. (1999) attenuation law $A_{UV} = 4.43 + 1.99\beta$, including the UV slope $\beta(M_{UV}, z)$ empirically from observations by Bouwens et al. (2014). We remove dust attenuation at $z > 10$ motivated by recent results suggesting dust attenuation is negligible in $z > 10$ galaxies (Topping et al. 2024a; Cullen et al. 2024; Morales et al. 2024), though we note that beyond $z \gtrsim 10$ dust has only a small impact on the UV LFs (Mason et al. 2023).

The resulting LFs for our mass-dependent UV scatter model are shown in Fig. 2 from $z = 5$ to 14. We compare them with the model without UV scatter (dashed lines), where the evolution of the LF directly follows the evolution of the underlying halo mass function. The solid curves are the LF obtained including the mass-dependent scatter $\sigma_{UV}(M_h)$ described in the previous section.

At progressively higher redshifts, the scatter in the UV luminosities has a stronger impact on the LF, which deviates more and more from the no-scatter case. The

presence of a UV scatter that decreases with halo mass *naturally produces* larger number densities of $M_{\rm UV} \lesssim -14$ galaxies at higher redshifts with respect to the no-scatter case. This is due to low mass halos (characterized by higher UV scatter) being progressively more dominant at earlier epochs.

As evident from the bottom right panel of Fig. 2 where we show the LFs up to fainter luminosities, the model also predicts a faint end turnover of the LF at magnitudes $M_{\rm UV} \gtrsim -13$. This is because we have imposed a cut-off in galaxy formation at the atomic cooling limit $M \sim 10^8 \, M_\odot$, i.e. lower mass halos cannot host a galaxy and thus will not be scattered up to populate the LF. While galaxies in higher mass halos are scattered down to lower luminosities during lulls in star formation, their number densities are lower than low mass halos, and they cannot boost the faint-end of the LF. If ever probed with deep observations (e.g. in lensed fields with JWST Atek et al. 2023b), this could provide an additional constraint on the dominant driver of star formation at high redshifts.

We find the mass-dependent UV scatter model successfully reproduces the observed HST and JWST up to $z \sim 12$ (Bouwens et al. 2022b; Finkelstein et al. 2023; Pérez-González et al. 2023; Donnan et al. 2024; McLeod et al. 2024), producing a ~ 1 dex increase in number densities of $M_{\rm UV} < -18$ galaxies at $z \gtrsim 9$ compared to the no-scatter model. The model slightly overpredicts the bright-end of the LF at $z \sim 8$, which is likely due to a combination of the dust modelling and the precise form of $\sigma_{\rm UV}(M_h)$. However, at redshifts greater than > 12, even the additional contribution from an enhanced UV scatter at low masses is not sufficient to reproduce the observed high number densities of galaxies. This suggests that additional physical processes may be at play at these redshifts to enhance the UV luminosities, as we will discuss in Sec. 4.

3.2. *Luminosity density evolution*

By integrating the LFs we derive the luminosity density $\rho_{\rm UV}$ for the mass-dependent UV scatter model, shown in Fig. 3 as a function of redshift. To be consistent with observations, we obtain $\rho_{\rm UV}$ by integrating the LFs down to a magnitude limit of $M_{\rm lim} = -17$. We also calculate the corresponding cosmic star formation rate density (SFRD) using the empirical relation $\mathrm{SFR}/(\mathrm{M_\odot \, yr^{-1}}) = 8 \times 10^{27} \mathrm{L}/(\mathrm{erg\, s^{-1} Hz^{-1}})$ from Madau et al. (1999).

The mass-dependent UV scatter and the no scatter models, shown with solid and dashed lines respectively, predict similar luminosity density at $z \sim 7$, but progressively diverge towards higher redshifts. While the
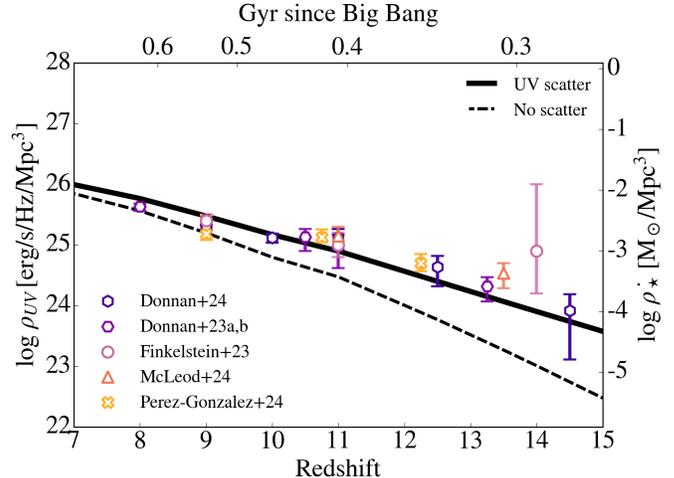
Figure 3. Luminosity density $\rho_{\rm UV}$ and cosmic star formation rate density SFRD as a function of redshift, derived integrating the UV LFs down to $M_{\rm lim} = -17$. The solid and dashed curves show the mass-dependent UV scatter and no-scatter models respectively. Also shown are observations from Bouwens et al. (2022a); Finkelstein et al. (2023); Pérez-González et al. (2023); Donnan et al. (2024); McLeod et al. (2024). We note that the apparent match to the observations at $z \sim 14$ is due to the steep faint-end slope of our LFs relative to that assumed by Donnan et al. (2024) (see Section 3.2).

no-scatter model underpredicts the observed luminosity density already from $z > 9$, the mass-dependent UV scatter model is in good agreement with the latest JWST observations up to $z \sim 11$, but then diverges from the observations at progressively earlier epochs.

We note that the luminosity density of the mass-dependent UV scatter model is consistent with the data from Donnan et al. (2024) up to $z \sim 14$, despite their LF exhibiting higher values at this redshift. This happens because their double power-law fit yields a shallower LF slope than our model towards fainter magnitudes, resulting in lower luminosity density when integrating up to $M_{\rm lim} = -17$. It is important to note that the luminosity density only reflects the integrated LF and caution should be taken when drawing conclusions based solely on its value. Therefore, while our luminosity density only slightly diverges from the data towards higher-z, this still suggests the need for extra luminosity production beyond that provided by stochastic star formation.

3.3. *Constraining the level of stochasticity*

Even if it cannot fully explain the number density of $z \gtrsim 12$ galaxies, bursty star formation still plays a role at cosmic dawn and it results from the complex interplay of multiple feedback processes acting on different timescales, which are not yet fully understood. Con-
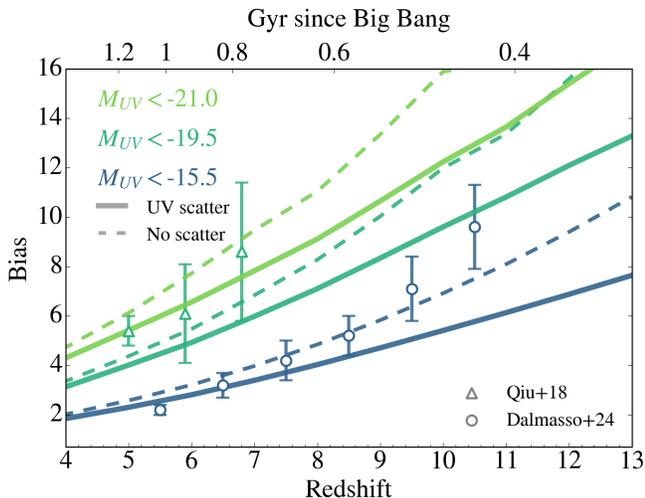
Figure 4. Redshift evolution of the predicted galaxy bias for the mass-dependent UV scatter model (solid lines) and the no-scatter model (dashed lines). Observations by Qiu et al. (2018) and Dalmasso et al. (2024a) are shown.

straining the level of stochasticity in galaxies would offer key insights into the physical and feedback processes driving the evolution of galaxies of different masses across cosmic time, and their associated timescales (e.g., Iyer et al. 2020).

However, the LF and luminosity density are intrinsically degenerate with respect to multiple physical effects, such as an enhancement of the star formation efficiency or of the UV scatter. As discussed by e.g., Mirocha (2020); Muñoz et al. (2023), this makes it impossible to use them alone as a tool to disentangle these physical processes. For this reason, it is important to identify additional key observables that can help us to independently constrain the importance of stochastic star formation at high-z.

To this aim, we discuss the expected implications of mass-dependent UV scatter on multiple quantities: galaxy clustering (Section 3.3.1), the evolution of the intergalactic medium (IGM) neutral fraction (Section 3.3.2), and spectral energy distributions (Section 3.3.3), providing predictions and tools to test the model against future observations.

3.3.1. *Clustering*

A key observational test of the importance of stochasticity in high-z galaxies is to connect galaxies to their dark matter halos. The clustering of galaxies is driven by the underlying distribution of the dark matter halos that they inhabit (see e.g., Wechsler & Tinker 2018, for a recent review). As discussed by Muñoz et al. (2023), constraints on galaxy clustering can thus break the degeneracies of the UVLF and distinguish the presence of

UV stochasticity from the effect of an increased average UV emission.

In a ΛCDM Universe, the galaxy bias (quantifying the halo-galaxy connection) is expected to increase with the halo mass: galaxies hosted by massive halos cluster more strongly than those residing in lower mass ones. Estimates of Lyman-break galaxy clustering at $z \sim 4-7$ have revealed the brightest galaxies tend to reside in the most massive halos (e.g., Barone-Nugent et al. 2014; Harikane et al. 2016, 2022; Qiu et al. 2018; Dalmasso et al. 2024b). As discussed by Muñoz et al. (2023), scatter in the $M_{UV} - M_h$ relation will lower the bias of galaxies, since UV luminous galaxies can be found in a broad range of halo masses.

It is therefore important to provide predictions for the galaxy bias in our mass-dependent UV-scatter model. We estimate the luminosity-weighted effective bias of galaxies as (see e.g., Muñoz et al. 2023):

$$b_{\mathrm{eff}}(M_{\mathrm{UV}}) = \frac{1}{\Phi(M_{\mathrm{UV}})} \int dM_h \, p(M_{\mathrm{UV}} \mid M_h) \frac{dn}{dM_h} b(M_h) \tag{3}$$

where we use the linear bias $b(M_h)$ fits from Tinker et al. (2010). Our predictions for the redshift evolution of the bias at fixed M_{UV} are shown in Fig. 4.

As expected, biases from the UV scatter model always have lower values than the no-scatter case, and the difference is progressively more pronounced towards higher redshifts as galaxies of fixed M_{UV} occupy lower mass halos. As discussed by Dalmasso et al. (2024b), measurements of galaxy bias are extremely challenging at high-z as estimates are limited by both Poisson noise due to low number counts and cosmic variance in small fields. Pre-JWST studies have measured the bias up to $z \sim 7$ for $M_{\mathrm{UV}} \lesssim -19$ galaxies, but the errors are too large to draw definite conclusions and constrain the models, as we can see when comparing our model with data from Qiu et al. (2018).

However, the sensitivity of JWST makes more accurate estimates of the bias feasible by enabling us to measure clustering for sub-$L^\star$ galaxies at $z > 6$ for the first time (e.g., Endsley et al. 2020; Dalmasso et al. 2024a). We compare our results with those of recent estimates from JWST/NIRCam observations of $M_{\mathrm{UV}} \lesssim -15$ galaxies at $z \sim 5-10$ in the GOODS-S field by Dalmasso et al. (2024a). The bias estimated by Dalmasso et al. (2024a) shows a very steep increase with redshift. At $z < 9$ the difference between our two models is too small to be probed by these observations. However, $z > 9$, the Dalmasso et al. (2024a) constraints are more consistent with the no-scatter case, and even slightly above both models at $z \sim 10$.

This could suggest galaxies experience a lower level of stochasticity than what we have assumed and/or are hosted in higher mass halos than expected at higher redshifts. This is somewhat surprising, as at fixed UV magnitude, models predict and clustering results imply that galaxies reside in lower mass halos at higher redshifts as star formation rates are higher (e.g., Mason et al. 2015; Tacchella et al. 2018; Harikane et al. 2022). This may potentially imply a change in the star formation efficiency with halo mass at high redshift.

However, we note that Dalmasso et al. (2024a) assumed a different cosmology than we have, and full interpretation of JWST observations likely requires a Halo Occupation Distribution (HOD) model approach (e.g., Harikane et al. 2022) to separate non-linear clustering on small scales due to satellite galaxies, as noted by Dalmasso et al. (2024a). In addition, large area, unbiased, surveys with JWST will be essential to constrain models by probing the number density and clustering of UV bright galaxies ($M_{\rm UV} \lesssim -20$) at $z \gtrsim 7$.

3.3.2. *Reionization history*

Constraints on the IGM reionization process offer vital information about star formation in *all* sources, even those too faint to detect directly with JWST. Muñoz et al. (2024) recently described how early JWST estimates of high ionizing photon production efficiency in high-z galaxies, taken at face-value, may imply a potential 'overproduction' of ionizing photons, which is at odds with current constraints on the timeline of reionization. Bursty star formation may alleviate this tension. In particular, Muñoz et al. (2024) assumed constant values of the ionizing photon escape fraction $f_{\rm esc}$ and ionizing photon production rate, $\xi_{\rm ion}$ at fixed $M_{\rm UV}$, which may not be realistic assumptions in a stochastic star formation scenario (see also Section 3.3.3).

Here, first, we discuss results from observations and simulations implying that ionizing photon production and escape may be linked to bursty star formation. Then, we combine our mass-dependent UV scatter model with simple models for $f_{\rm esc}$ and $\xi_{\rm ion}$ as a function to offset from the median $M_{\rm UV,c}(M_h)$ relation to explore how bursty star formation impacts the reionization history.

Observationally, high ionizing photon production rate ($\xi_{\rm ion}$) is linked to high equivalent width nebular emission lines, and thus young, massive stars (e.g., Chevallard et al. 2018; Tang et al. 2019, 2021). Therefore, if galaxies undergo bursty star formation, the number of ionizing photons they produce will vary significantly throughout their star formation history. Indeed, as discussed in the introduction, Endsley et al. (2023b) recently found

that UV-faint galaxies ($M_{\rm UV} \gtrsim -17$) are more likely to have weaker nebular emission lines and be experiencing a down-turn in star formation compared to UV-bright galaxies ($M_{\rm UV} \lesssim -20$). Endsley et al. (2023b) discuss that one interpretation of the weaker emission lines in UV-faint galaxies is due to their star formation histories (rather than an increase in $f_{\rm esc}$ in faint galaxies, which produces a degenerate effect in photometric data). In this case, they find $\xi_{\rm ion}$ is a broad distribution that can be strongly dependent on UV magnitude.

Furthermore, hydrodynamical simulations predict that the escape fraction of ionizing photons may also coincide with (or shortly after) star formation bursts (Kimm & Cen 2014; Paardekooper et al. 2015; Ma et al. 2020a; Barrow et al. 2020). In particular, hard radiation from massive stars may allow ionizing photons to escape by creating 'porous' density-bounded HII regions and/or stellar winds or supernovae feedback can open low-density channels (e.g., Zackrisson et al. 2013; Steidel et al. 2018). From the observational side, this picture is not completely clear: while many Lyman-continuum leakers detected at $z \sim 0.3 - 0.4$ are in a period of intense star formation, with specific star formation rates $\gtrsim 10 \, {\rm Gyr}^{-1}$ and star formation rate surface densities $\Sigma_{\rm SFR} \gtrsim 10 \, M_\odot \, {\rm yr}^{-1} \, {\rm kpc}^{-2}$ (e.g., Izotov et al. 2016, 2018; Flury et al. 2022), observations at $z \sim 3$ show no clear trend of $f_{\rm esc}$ with specific star formation rate, age or $\Sigma_{\rm SFR}$ (Pahl et al. 2022, 2023).

In the context of our mass-dependent UV scatter model, we combine these observational and theoretical insights with our UV LFs to assess the impact of stochasticity on the timeline of reionization. In particular, as discussed by Tang et al. (2019), Naidu et al. (2022) and Endsley et al. (2023b), among others, we consider that galaxies experiencing a burst of star formation, i.e. that will be up-scattered in the $M_{\rm UV} - M_h$ distribution, could have an outsized contribution to the ionizing photon budget.

This effect can be translated into $\xi_{\rm ion}$ and $f_{\rm esc}$ being described by a distribution at fixed UV magnitudes rather than fixed values for every galaxy. The production rate of ionizing photons available for reionization can therefore be expressed as:

$$\dot{n}_{\rm ion}(z) = \int_{-\infty}^{M_{lim}} dM_{\rm UV} L(M_{\rm UV}) \Phi(M_{\rm UV})$$
$$\times f_{\rm esc} \xi_{\rm ion} \, p(f_{\rm esc}, \xi_{\rm ion} \mid M_{\rm UV}); \quad (4)$$

which can be solved when an empirical relation between $\xi_{\rm ion}$ and $M_{\rm UV}$ is available.

Within our modeling framework, we model $\xi_{\rm ion}$ and $f_{\rm esc}$ as functions of $\Delta M_{\rm UV} = M_{\rm UV,c}(M_h) - M_{\rm UV}$. As illustrated in the middle panel of Fig. 5, we assume
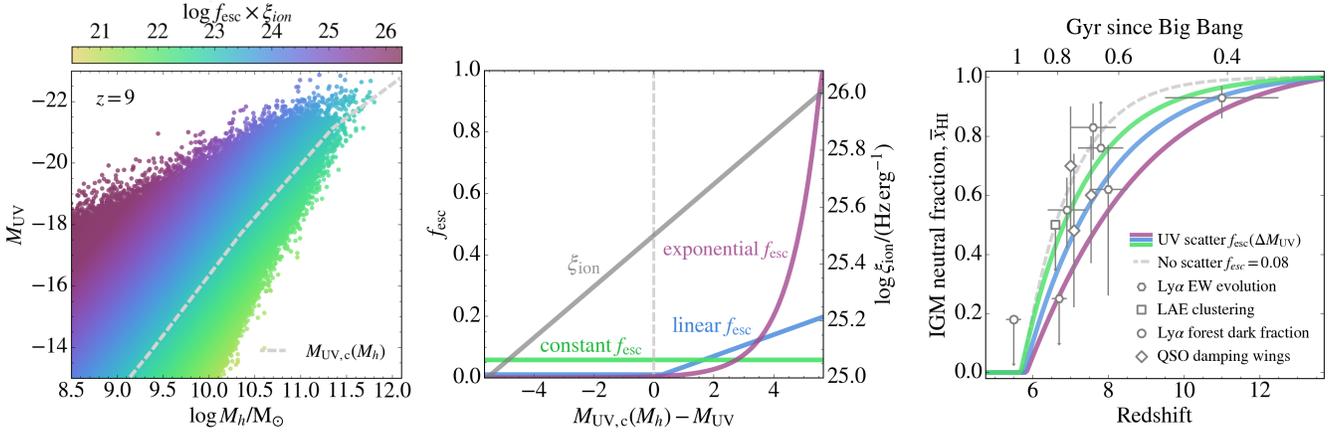
Figure 5. *Left*: $M_{UV} - M_h$ relation at $z = 9$, populated with galaxies following the halo mass function and coloured with the product $f_{esc}\xi_{ion}$ (assuming an exponentially increasing f_{esc} and linearly increasing ξ_{ion} with ΔM_{UV}), showing how up-scattered galaxies will contribute the most to the number density of ionizing photons. *Centre*: escape fraction f_{esc} and ionising photon production efficiency ξ_{ion} as a function of ΔM_{UV}. For the escape fraction we show three different cases of constant, linear and exponential increase towards up-scattered galaxies. *Right*: Redshift evolution of the fraction of neutral hydrogen in the IGM for the same three scenarios, as well as for the case without scatter, assuming fixed $f_{esc} = 0.08$ and $\log_{10} \xi_{ion}/(\mathrm{Hz\,erg}^{-1}) = 25.7$. We also plot measurements from observations of: the evolution of the Lyα equivalent width (EW, Mason et al. 2018, 2019; Bolan et al. 2022), the clustering of Lyα emitters (LAE, Ouchi et al. 2010; Sobacchi & Mesinger 2015), Lyα forest dark pixel fraction (McGreer et al. 2015), and quasar damping wings (Davies et al. 2018; Greig et al. 2019).

$\log_{10} \xi_{ion}$ increases linearly with ΔM_{UV}, which naturally produces a log-normal distribution of $p(\xi_{ion} \mid M_{UV})$, similar to observations (e.g., Prieto-Lyon et al. 2023; Endsley et al. 2023b). For the escape fraction we explore three different scenarios: (i) exponentially increasing $f_{esc}(\Delta M_{UV})$, which produces an exponential distribution of $p(f_{esc} \mid M_{UV})$ (similar to that derived for $z \sim 3.5$ star forming galaxies by Kreilgaard et al. 2024); (ii) linearly increasing $f_{esc}(\Delta M_{UV})$; and (iii) constant $f_{esc}(\Delta M_{UV})$ for all galaxies.

In Fig. 5, left, we show the $M_{UV} - M_h$ relation at $z = 9$, populated following the halo mass function and our mass-dependent $\sigma_{UV}(M_h)$ model. Each galaxy is coloured with the corresponding product of escape fraction and ionizing efficiency for the exponentially increasing f_{esc} case.

Using these assumptions, we can derive $\dot{n}_{ion}(z)$ as:

$$\dot{n}_{ion}(z) = \int_{-\infty}^{M_{lim}} dM_{UV} L(M_{UV}) \Phi(M_{UV})$$

$$\times \int_{M_{h,min}}^{\infty} dM_h \, f_{esc}[\Delta M_{UV}(M_h)] \, \xi_{ion}[(\Delta M_{UV}(M_h)]$$

$$\times \, p(M_{UV} \mid M_h) \frac{dn}{dM_h}; \quad (5)$$

where we set $M_{lim} = -13$, but note that our results are relatively insensitive to the exact value of this choice due to the turn-over of the UV scatter LFs at $M_{UV} \sim -13$ (Fig. 2). The ionizing photon rate production can be then used to calculate the cosmic evolution of the ionized

hydrogen fraction by solving Eq. (6) in Mason et al. (2015).

The resulting reionization histories for the three scenarios are shown on the right of Fig. 5. We also compare to the no-scatter case, for which we assume fixed f_{esc} and $\xi_{ion} = 10^{25.7} \mathrm{Hz\,erg}^{-1}$ (consistent with the latest JWST results; e.g. Endsley et al. 2023a; Atek et al. 2024). For each model, f_{esc} is tuned to obtain the end of reionization by $z \lesssim 6$, as inferred from Lyman-alpha forest observations (Qin et al. 2021; Bosman et al. 2022; Jin et al. 2023). In the no-scatter scenario this leads to a value of $f_{esc} = 0.08$. As discussed by Muñoz et al. (2024) this may be in tension with estimates from low-z analogs which would predict higher f_{esc}.

When adding stochastic star formation, we obtain an earlier onset and more gradual evolution of reionization, as low mass halos can start producing significant ionizing photons at early times (see also Furlanetto & Mirocha 2022). We find the shape of the reionization timeline is strongly dependent on our f_{esc} model. The steeper the dependency of f_{esc} with $\Delta M_{UV}(M_h)$ (i.e. going from the constant to the exponential scenario), the earlier the start and the shallower the evolution of the reionization process.

At face-value, stochastic star formation exacerbates the potential ionizing photon crisis: due to the higher luminosity densities in our scatter model, we require an even lower value of $f_{esc} \sim 0.05$ than the no-scatter case ($f_{esc} \sim 0.08$) to obtain a $z \sim 6$ end of reionization. We note here that our linear ξ_{ion} model also assumes ξ_{ion}

is higher for starbursting galaxies, but even when using a constant $\xi_{\rm ion}$ model the higher luminosity density of the scatter model implies a higher injection rate of ionizing photons at $z \gtrsim 8$ compared to the no-scatter case. This motivates the need to consider a distribution of escape fractions and $\xi_{\rm ion}$, different for galaxies in different stages of their bursty SFH, to properly model early galaxies' contribution to reionization.

We note however that while there are observational constraints on $\xi_{\rm ion}$ at high-z, the escape fraction is not directly constrained. Thus our predictions here are merely illustrative, but demonstrate that stochasticity can have a marked impact on the timing of reionization and is an important additional constraint to understand early star formation, and can be constrained now to $z \gtrsim 10$ with JWST observations (e.g., Nakane et al. 2023; Umeda et al. 2023).

As stochasticity implies lower mass halos (which are less biased, see above) are more important for reionization this would also impact the morphology of reionization. We would expect more numerous, smaller bubbles at fixed neutral fraction compared to a case with no stochasticity (e.g. Hutter et al. 2021, 2023; Lu et al. 2024). This could potentially be measured via Lyman-alpha transmission and 21-cm intensity mapping.

3.3.3. *Spectral Energy Distributions*

Highly time variable, bursty star formation histories that can produce drastic variability of the luminosity of a galaxy across its evolution, should also cause large scatter in galaxies' spectral features when we observe galaxies at fixed $M_{\rm UV}$ or stellar mass, as we are observing galaxies at different phases in their SFHs (e.g. Iyer et al. 2024; Sun et al. 2023a; Endsley et al. 2023b). Different spectral features are sensitive to different timescales and galaxy properties, and are commonly used to probe galaxy star formation histories (e.g. Weisz et al. 2012; Sparre et al. 2017; Ciesla et al. 2023; Cole et al. 2023; Topping et al. 2024a; Langeroodi & Hjorth 2024). In the context of understanding the role of stochasticity at high-z it is important to identify which are the best observable features to help us constrain stochasticity

JWST makes it possible to measure variations across galaxy populations at $z \sim 5 - 15$. Several recent works have quantified stochasticity at $z \gtrsim 5$ via the scatter in the star-formation main sequence using JWST photometry (SFR - stellar mass, e.g., Ciesla et al. 2023; Cole et al. 2023; Caputi et al. 2023), finding evidence for a potential increase in scatter with increasing redshift. However, it becomes increasingly challenging to measure accurate stellar masses from photometry for

bursty galaxies, due to the 'outshining' of rest-optical stellar emission by nebular emission from younger stars (e.g., Stark et al. 2013; Whitler et al. 2023; Giménez-Arteaga et al. 2023; Narayanan et al. 2024). Analyses at fixed UV magnitude may provide more reliable comparisons with models during this bursty epoch of galaxy formation (e.g., Endsley et al. 2023b).

To this aim, we explore the impact of simple bursty star formation histories on galaxy SEDs at fixed $M_{\rm UV}$, to avoid the issues of stellar mass uncertainties.

Following Mason et al. (2015), we set the average star formation rate of a halo of mass M_h as $\langle {\rm SFR} \rangle \propto \epsilon_\star(M_h)\,f_b M_h$. On top of this constant evolution we artificially add a "burstiness" by modeling the SFH as a periodic pattern in which burst-phases and lull-phases alternates. Specifically the SFR varies between $\log\langle {\rm SFR} \rangle + \Delta \log {\rm SFR}$, during bursts, and $\log\langle {\rm SFR} \rangle - \Delta \log {\rm SFR}$, during lulls. The value of $\Delta {\rm SFR}$ and the duration of burst and lull phases is calibrated so that the stellar mass assembled over the total period remains the same as for the constant evolution.

To check how this burstiness affects the emission of galaxies, we produce synthetic continuum SEDs. We sample the SFH as a series of single bursts every 1 Myr and use STARBURST99 (Leitherer et al. 1999) with PADOVA stellar tracks (Bertelli et al. 1994) and assuming a Kroupa (2001) initial mass function between 0.1 and 100 $M_\odot$ to derive the rest-frame spectra and $M_{\rm UV}$ (see also Gelli et al. 2021).

We then select galaxies at the same magnitude $M_{\rm UV}$, finding that they can show a wide range of different SFH and properties due to their stochastic behaviour.

In Fig. 6, left panel, we show as an example the SFHs of three galaxies with same magnitude $M_{\rm UV} = -20$ at $z = 10$, but hosted in halos of different mass. The one in the lowest mass halos is experiencing a burst of star formation, and is therefore up-scattered in the $M_{\rm UV} - M_h$ relation, whereas the ones in higher mass halo are in a lull phase.

In the right panel of Fig. 6 we show with the same color coding their redshifted observed flux $z = 10$. By definition, their rest-frame 1500Å luminosity is the same, but we can see that significant differences are present in their UV slopes β_{UV} and Balmer breaks at $\lambda_{rest} \sim 3645$Å. Galaxies experiencing a recent rise in the SFR have steeper UV slopes, since their emission is dominated by young massive stars. On the other hand, galaxies undergoing a constant or recently decreasing period of SFR have shallower UV slopes and much more prominent Balmer breaks.

While not modelled here, we also expect the strength of nebular emission lines that trace star formation on
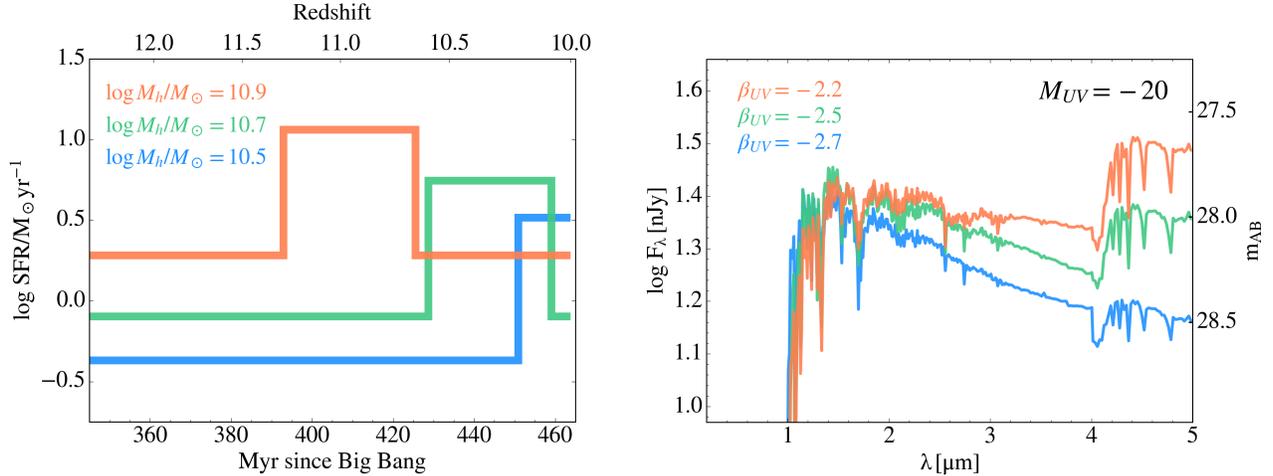
Figure 6. Examples of star formation histories (*left*) and continuum spectral energy distributions (*right*) for three galaxies at $z = 10$ with same UV magnitude $M_{UV} = -20$.

short timescales (< 10 Myr), such as $H\alpha$, to be enhanced during bursty phases (see e.g., Weisz et al. 2012; Sparre et al. 2017). As a consequence, the β_{UV}, Balmer breaks and line equivalent widths represent quantities that can give us precious direct insight on bursty star formation (see also e.g. Endsley et al. 2023b; Trussler et al. 2024; Langeroodi & Hjorth 2024; Topping et al. 2024a). Larger samples of galaxies are expected to show wide distributions of these quantities at fixed magnitude. In a forthcoming work, we will extend our predictions, analyzing in detail the expected distributions of β_{UV} slopes and Balmer breaks, as well as of emission line equivalent widths and other spectral features, all essential to constrain the bursty behavior of high-z galaxies and to infer the timescales and physical processes regulating them.

4. DISCUSSION: THE ABUNDANCE OF GALAXIES AT $Z > 12$

Despite the success of the mass-dependent UV scatter model in naturally producing higher UVLFs at progressively higher redshifts, it still cannot reproduce the observed high number densities of galaxies at $z > 12$.

Our analysis was based on some fundamental assumptions regarding: (i) the cosmological parameters, (ii) the halo mass function, and (iii) the form used for the matter transfer function. We tested how these assumptions impact the predicted LFs in Appendix A, and find that their effect is mostly negligible (with some exception for the transfer function).

Thus, the persisting discrepancy at $z > 12$ suggests that stochastic star formation alone is not sufficient to fill the gap and that additional physical processes may be at play.

As mentioned in the introduction, another way to boost the abundance of high-z galaxies is through an enhancement of the average $M_{UV} - M_h$ relation. This could be achieved if galaxies are forming stars in a more efficient manner at high-z. Our model currently employs a redshift independent star formation efficiency, a strong assumption that likely needs to be relaxed to match the $z > 12$ observations.

The fact that our model reflects a stochasticity proportional to the inverse of the halo escape velocity offers an interesting insight. As $v_{\rm esc} \sim M_h^{1/3}(1+z)^{1/2}$ we should expect a *decrease* in stochasticity at fixed halo mass at higher redshifts, as halos are more compact and thus better able to retain their gas. This implies higher redshift halos should host higher gas masses at fixed halo mass, which may provide fuel for more efficient star formation.

As proposed by Dekel et al. (2023), a possible cause for higher star formation efficiency at high redshift is an increase in the density of star forming regions. Cloud-scale simulations show that when a surface density threshold is reached ($\Sigma \gtrsim 10^3 \, M_\odot \, {\rm pc}^{-2}$) stellar feedback may not be fast enough to counteract gravitational collapse and the star formation efficiency can be extremely enhanced from usual values of $\lesssim 10\%$ to $\sim 100\%$ (e.g. Grudić et al. 2018; Lancaster et al. 2021; Menon et al. 2023, 2024). Galaxy-scale hydrodynamic simulations show that to create such high density clouds likely requires a turbulent gas-rich environment where gas is compressed by feedback-driven winds and shocks from inflowing gas (Ma et al. 2020b). Dekel et al. (2023) and Li et al. (2023) discuss that we may expect more galaxies at high redshift to satisfy these high star formation efficiency conditions as halos become increasingly compact and accretion rates increase.

Indeed, observations show galaxies appear to be increasingly compact at $z > 4$ (e.g. Langeroodi & Hjorth 2023; Morishita et al. 2024). Furthermore, extremely high electron densities ($n_e \gtrsim 10^4$ cm^{-3}) have been detected in two UV-bright, compact $z \gtrsim 6$ sources (GNz11 and RXCJ2248-ID) which show UV emission line signatures of massive stars (Senchyna et al. 2023; Topping et al. 2024b, though c.f. Maiolino et al. 2023 where the high electron density of GNz11 is attributed to an AGN broad-line region). Topping et al. (2024a) suggest such high electron densities could result from the high density birth clouds described above, which can fuel efficient star formation. Larger samples of $z > 6$ sources with deep, high-resolution rest-UV spectroscopy trace both massive star signatures and ionized gas densities, combined with morphological information, should enable a better understanding of the links between efficient star formation and high densities.

5. CONCLUSIONS

We have explored the impact of a mass-dependent scatter of the $M_{\rm UV} - M_h$ relation on the UV luminosity functions of high-z galaxies, and other observables, to understand the relevance of bursty star formation in the early Universe. We assumed a decreasing trend $\sigma_{\rm UV}(M_h) \sim M_h^{-1/3}$ with increasing M_h, reflecting the higher sensitivity of low-mass halos to stochastic star formation processes due to their lower halo escape velocities. Our main conclusions are the following:

- The mass-dependent UV scatter model naturally produces higher UV LFs at progressively higher redshifts with respect to the no-stochasticity case, due to low-mass halos being more dominant at earlier epochs;

- The predicted LF and luminosity density are in agreement with the latest JWST observations up to $z \sim 12$, but start to diverge at progressively earlier epochs, suggesting the need for additional UV luminosity production on top of that provided by stochastic star formation. This may be linked to the increasing compactness, and thus density, of halos at fixed mass with redshift;

- The model predicts significantly lower galaxy bias values than the no-scatter case as a function of

redshift, with the models diverging at $z \gtrsim 8$ for $M_{\rm UV} \sim -21$ galaxies;

- Assuming that up-scattered galaxies are the dominant source of ionizing photons yields an earlier start to reionization and a more gradual reionization timeline than a model without scatter;
- Balmer breaks, nebular emission line strengths and UV-slopes are also sensitive to bursty star formation histories and can have significantly different values for galaxies with same $M_{\rm UV}$.

Our results show that bursty star formation leading to a mass-dependent stochasticity in the UV luminosity - halo mass relation is expected to have an impact on multiple observable quantities. JWST observations are probing the high-z UV luminosity functions with increasing depth and precision, but, as discussed by Muñoz et al. (2023), the contribution of bursty star formation cannot be constrained by the LF alone due to degeneracies with other physical effects. For this reason, it is essential to use multiple independent observables simultaneously to definitively understand the role of bursty star formation in high-z galaxies' evolution (see also e.g., Mirocha & Furlanetto 2023; Endsley et al. 2023b; Topping et al. 2024a; Langeroodi & Hjorth 2024; Trussler et al. 2024).

Since our model assumes a redshift-independent star formation efficiency and still struggles to reproduce the extremely high redshift observations at $z > 12$, there is a clear need for further investigation of the physics of the earliest galaxies to understand how they formed the first stellar populations.

APPENDIX

A. THE IMPACT OF COSMOLOGICAL ASSUMPTIONS ON THE UVLF

To make our predictions for the UVLFs, we had to make some assumptions regarding: (i) the cosmological parameters, (ii) the halo mass function, and (iii) the form used for the matter transfer function. Previous work modelling high-z LFs have assumed a variety of choices for the above. To assess the impact of these choices on our results, we have tested our UV-scatter model results varying these set of assumptions one at a time.

By changing the cosmological parameters from those of a flat ΛCDM with $\Omega_m = 0.3$, $\Omega_\Lambda = 0.7$ and $h = 0.7$, to the Planck Collaboration et al. (2020) measurements through the cosmic microwave background (CMB) anisotropies ($\Omega_m = 0.315$, $\Omega_\Lambda = 0.685$ and $h = 0.67$), we find a completely negligible change in the LF.

For the HMF, we use the HMF python package by Murray et al. (2013) and assumed a Reed et al. (2007) function, which had been simulated specifically for halos at $z \sim 10 - 30$. Using instead the functions from Sheth et al. (2001) and Behroozi et al. (2013) results in slightly higher and lower number densities respectively, with the maximum change produced in the LFs of ~ 0.5 dex (see Figure 7, left panel). We can conclude that the choice of the HMF produces a minor effect on the LFs, but that our overall conclusions do not depend on its choice.

Finally, we test the impact of the assumed linear transfer function by changing it from the Eisenstein & Hu (1998) form to the one calculated with the Code for Anisotropies in the Microwave Background (CAMB, Lewis et al. 2000), both included in the HMF package. This time, the change in the LFs is significant, especially towards the faint end, with the LF being higher by up to ~ 1 dex when using CAMB. This could be linked to an excess of the power spectrum at very small scales in the CAMB function implementation, and/or possibly due to the default extrapolation of the CAMB transfer function at high wavenumber in the HMF code[3]. We therefore caution that care must be taken when using the default CAMB option for the transfer function in HMF as it can lead to an overestimation of the LF at high-z.
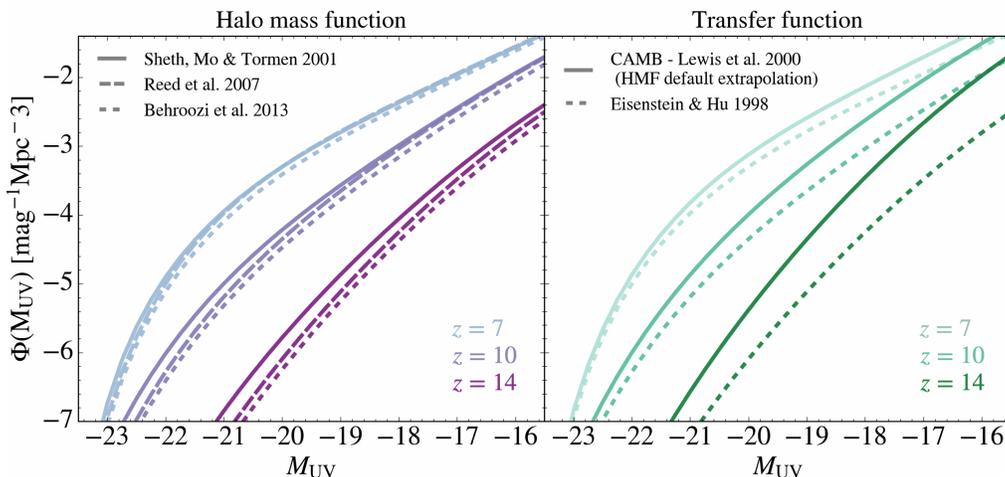
Figure 7. UVLF at $z = 7, 10, 14$ for different halo mass functions (*left*) and transfer functions (*right*).

REFERENCES

Adams, N. J., Conselice, C. J., Ferreira, L., et al. 2023, MNRAS, 518, 4755, doi: 10.1093/mnras/stac3347

Atek, H., Shuntov, M., Furtak, L. J., et al. 2023a, MNRAS, 519, 1201, doi: 10.1093/mnras/stac3144

Atek, H., Chisholm, J., Alavi, A., et al. 2023b, JWST's GLIMPSE: gravitational lensing & NIRCam imaging to probe early galaxy formation and sources of reionization, JWST Proposal. Cycle 2, ID. #3293

Atek, H., Labbé, I., Furtak, L. J., et al. 2024, Nature, 626, 975, doi: 10.1038/s41586-024-07043-6

Barone-Nugent, R. L., Trenti, M., Wyithe, J. S. B., et al. 2014, ApJ, 793, 17, doi: 10.1088/0004-637X/793/1/17

Barrow, K. S. S., Robertson, B. E., Ellis, R. S., et al. 2020, ApJL, 902, L39, doi: 10.3847/2041-8213/abbd8e

[3] https://github.com/halomod/hmf/issues/90

Behroozi, P. S., Wechsler, R. H., & Conroy, C. 2013, ApJ, 770, 57, doi: 10.1088/0004-637X/770/1/57

Bertelli, G., Bressan, A., Chiosi, C., Fagotto, F., & Nasi, E. 1994, A&A Supp., 106, 275

Bolan, P., Lemaux, B. C., Mason, C., et al. 2022, MNRAS, 517, 3263, doi: 10.1093/mnras/stac1963

Bosman, S. E. I., Davies, F. B., Becker, G. D., et al. 2022, MNRAS, 514, 55, doi: 10.1093/mnras/stac1046

Bouwens, R. J., Illingworth, G., Ellis, R. S., Oesch, P., & Stefanon, M. 2022a, ApJ, 940, 55, doi: 10.3847/1538-4357/ac86d1

Bouwens, R. J., Illingworth, G. D., Oesch, P. A., et al. 2014, ApJ, 793, 115, doi: 10.1088/0004-637X/793/2/115

Bouwens, R. J., Smit, R., Schouws, S., et al. 2022b, ApJ, 931, 160, doi: 10.3847/1538-4357/ac5a4a

Bouwens, R. J., Stefanon, M., Brammer, G., et al. 2023, MNRAS, 523, 1036, doi: 10.1093/mnras/stad1145

Bromm, V., & Yoshida, N. 2011, ARA&A, 49, 373, doi: 10.1146/annurev-astro-081710-102608

Caputi, K. I., Rinaldi, P., Iani, E., et al. 2023, arXiv e-prints, arXiv:2311.12691, doi: 10.48550/arXiv.2311.12691

Castellano, M., Fontana, A., Treu, T., et al. 2022, ApJL, 938, L15, doi: 10.3847/2041-8213/ac94d0

Chevallard, J., Charlot, S., Senchyna, P., et al. 2018, MNRAS, 479, 3264, doi: 10.1093/mnras/sty1461

Ciesla, L., Elbaz, D., Ilbert, O., et al. 2023, arXiv e-prints, arXiv:2309.15720, doi: 10.48550/arXiv.2309.15720

Cole, J. W., Papovich, C., Finkelstein, S. L., et al. 2023, arXiv e-prints, arXiv:2312.10152, doi: 10.48550/arXiv.2312.10152

Cullen, F., McLeod, D. J., McLure, R. J., et al. 2024, MNRAS, doi: 10.1093/mnras/stae1211

Curti, M., Maiolino, R., Curtis-Lake, E., et al. 2023, arXiv e-prints, arXiv:2304.08516, doi: 10.48550/arXiv.2304.08516

Dalmasso, N., Leethochawalit, N., Trenti, M., & Boyett, K. 2024a, arXiv e-prints, arXiv:2402.18052, doi: 10.48550/arXiv.2402.18052

Dalmasso, N., Trenti, M., & Leethochawalit, N. 2024b, MNRAS, 528, 898, doi: 10.1093/mnras/stad3901

Davies, F. B., Hennawi, J. F., Bañados, E., et al. 2018, ApJ, 864, 142, doi: 10.3847/1538-4357/aad6dc

Dekel, A., Sarkar, K. C., Birnboim, Y., Mandelker, N., & Li, Z. 2023, MNRAS, 523, 3201, doi: 10.1093/mnras/stad1557

Dome, T., Tacchella, S., Fialkov, A., et al. 2023, arXiv e-prints, arXiv:2305.07066, doi: 10.48550/arXiv.2305.07066

Donnan, C. T., McLure, R. J., Dunlop, J. S., et al. 2024, arXiv e-prints, arXiv:2403.03171, doi: 10.48550/arXiv.2403.03171

Eisenstein, D. J., & Hu, W. 1998, ApJ, 496, 605, doi: 10.1086/305424

Endsley, R., Behroozi, P., Stark, D. P., et al. 2020, MNRAS, 493, 1178, doi: 10.1093/mnras/staa324

Endsley, R., Stark, D. P., Whitler, L., et al. 2023a, MNRAS, 524, 2312, doi: 10.1093/mnras/stad1919

—. 2023b, arXiv e-prints, arXiv:2306.05295, doi: 10.48550/arXiv.2306.05295

Ferrara, A. 2023, arXiv e-prints, arXiv:2310.12197, doi: 10.48550/arXiv.2310.12197

Finkelstein, S. L., Leung, G. C. K., Bagley, M. B., et al. 2023, arXiv e-prints, arXiv:2311.04279, doi: 10.48550/arXiv.2311.04279

Fiore, F., Ferrara, A., Bischetti, M., Feruglio, C., & Travascio, A. 2023, ApJL, 943, L27, doi: 10.3847/2041-8213/acb5f2

Flury, S. R., Jaskot, A. E., Ferguson, H. C., et al. 2022, ApJ, 930, 126, doi: 10.3847/1538-4357/ac61e4

Furlanetto, S. R., & Mirocha, J. 2022, MNRAS, 511, 3895, doi: 10.1093/mnras/stac310

Gelli, V., Salvadori, S., Ferrara, A., & Pallottini, A. 2024, ApJ, 964, 76, doi: 10.3847/1538-4357/ad23ec

Gelli, V., Salvadori, S., Ferrara, A., Pallottini, A., & Carniani, S. 2021, ApJL, 913, L25, doi: 10.3847/2041-8213/abfe6c

—. 2023, ApJL, 954, L11, doi: 10.3847/2041-8213/acee80

Gelli, V., Salvadori, S., Pallottini, A., & Ferrara, A. 2020, MNRAS, 498, 4134, doi: 10.1093/mnras/staa2410

Giménez-Arteaga, C., Oesch, P. A., Brammer, G. B., et al. 2023, ApJ, 948, 126, doi: 10.3847/1538-4357/acc5ea

Greig, B., Mesinger, A., & Bañados, E. 2019, MNRAS, 484, 5094, doi: 10.1093/mnras/stz230

Grudić, M. Y., Hopkins, P. F., Faucher-Giguère, C.-A., et al. 2018, MNRAS, 475, 3511, doi: 10.1093/mnras/sty035

Harikane, Y., Ouchi, M., Ono, Y., et al. 2016, ApJ, 821, 123, doi: 10.3847/0004-637X/821/2/123

Harikane, Y., Ono, Y., Ouchi, M., et al. 2022, ApJS, 259, 20, doi: 10.3847/1538-4365/ac3dfc

Harikane, Y., Ouchi, M., Oguri, M., et al. 2023, ApJS, 265, 5, doi: 10.3847/1538-4365/acaaa9

Hopkins, P. F., Gurvich, A. B., Shen, X., et al. 2023, MNRAS, 525, 2241, doi: 10.1093/mnras/stad1902

Hutter, A., Dayal, P., Legrand, L., Gottlöber, S., & Yepes, G. 2021, MNRAS, 506, 215, doi: 10.1093/mnras/stab877

Hutter, A., Trebitsch, M., Dayal, P., et al. 2023, MNRAS, 524, 6124, doi: 10.1093/mnras/stad2230

Inayoshi, K., Harikane, Y., Inoue, A. K., Li, W., & Ho, L. C. 2022, ApJL, 938, L10, doi: 10.3847/2041-8213/ac9310

Iyer, K. G., Speagle, J. S., Caplar, N., et al. 2024, ApJ, 961, 53, doi: 10.3847/1538-4357/acff64

Iyer, K. G., Tacchella, S., Genel, S., et al. 2020, MNRAS, 498, 430, doi: 10.1093/mnras/staa2150

Izotov, Y. I., Schaerer, D., Thuan, T. X., et al. 2016, MNRAS, 461, 3683, doi: 10.1093/mnras/stw1205

Izotov, Y. I., Worseck, G., Schaerer, D., et al. 2018, MNRAS, 478, 4851, doi: 10.1093/mnras/sty1378

Jin, X., Yang, J., Fan, X., et al. 2023, ApJ, 942, 59, doi: 10.3847/1538-4357/aca678

Kimm, T., & Cen, R. 2014, ApJ, 788, 121, doi: 10.1088/0004-637X/788/2/121

Kravtsov, A., & Belokurov, V. 2024, arXiv e-prints, arXiv:2405.04578, doi: 10.48550/arXiv.2405.04578

Kreilgaard, K. C., Mason, C. A., Cullen, F., Begley, R., & McLure, R. J. 2024. https://arxiv.org/abs/2405.10364

Kroupa, P. 2001, MNRAS, 322, 231, doi: 10.1046/j.1365-8711.2001.04022.x

Lancaster, L., Ostriker, E. C., Kim, J.-G., & Kim, C.-G. 2021, ApJL, 922, L3, doi: 10.3847/2041-8213/ac3333

Langeroodi, D., & Hjorth, J. 2023, arXiv e-prints, arXiv:2307.06336, doi: 10.48550/arXiv.2307.06336

—. 2024, arXiv e-prints, arXiv:2404.13045, doi: 10.48550/arXiv.2404.13045

Legrand, L., Hutter, A., Dayal, P., et al. 2022, MNRAS, 509, 595, doi: 10.1093/mnras/stab3034

Leitherer, C., Schaerer, D., Goldader, J. D., et al. 1999, ApJS, 123, 3, doi: 10.1086/313233

Lewis, A., Challinor, A., & Lasenby, A. 2000, ApJ, 538, 473, doi: 10.1086/309179

Li, Z., Dekel, A., Sarkar, K. C., et al. 2023, arXiv e-prints, arXiv:2311.14662, doi: 10.48550/arXiv.2311.14662

Looser, T. J., D'Eugenio, F., Maiolino, R., et al. 2023a, arXiv e-prints, arXiv:2302.14155. https://arxiv.org/abs/2302.14155

—. 2023b, arXiv e-prints, arXiv:2306.02470, doi: 10.48550/arXiv.2306.02470

Lu, T.-Y., Mason, C. A., Hutter, A., et al. 2024, MNRAS, 528, 4872, doi: 10.1093/mnras/stae266

Ma, X., Quataert, E., Wetzel, A., et al. 2020a, MNRAS, 498, 2001, doi: 10.1093/mnras/staa2404

Ma, X., Hopkins, P. F., Garrison-Kimmel, S., et al. 2018, MNRAS, 478, 1694, doi: 10.1093/mnras/sty1024

Ma, X., Grudić, M. Y., Quataert, E., et al. 2020b, MNRAS, 493, 4315, doi: 10.1093/mnras/staa527

Madau, P., Haardt, F., & Rees, M. J. 1999, ApJ, 514, 648, doi: 10.1086/306975

Maiolino, R., Scholtz, J., Witstok, J., et al. 2023, arXiv e-prints, arXiv:2305.12492, doi: 10.48550/arXiv.2305.12492

Mason, C. A., Trenti, M., & Treu, T. 2015, ApJ, 813, 21, doi: 10.1088/0004-637X/813/1/21

—. 2023, MNRAS, 521, 497, doi: 10.1093/mnras/stad035

Mason, C. A., Treu, T., Dijkstra, M., et al. 2018, ApJ, 856, 2, doi: 10.3847/1538-4357/aab0a7

Mason, C. A., Fontana, A., Treu, T., et al. 2019, MNRAS, 485, 3947, doi: 10.1093/mnras/stz632

McGreer, I. D., Mesinger, A., & D'Odorico, V. 2015, MNRAS, 447, 499, doi: 10.1093/mnras/stu2449

McLeod, D. J., Donnan, C. T., McLure, R. J., et al. 2024, MNRAS, 527, 5004, doi: 10.1093/mnras/stad3471

Menon, S. H., Federrath, C., & Krumholz, M. R. 2023, MNRAS, 521, 5160, doi: 10.1093/mnras/stad856

Menon, S. H., Lancaster, L., Burkhart, B., et al. 2024, arXiv e-prints, arXiv:2405.00813, doi: 10.48550/arXiv.2405.00813

Meurer, G. R., Heckman, T. M., & Calzetti, D. 1999, ApJ, 521, 64, doi: 10.1086/307523

Mirocha, J. 2020, MNRAS, 499, 4534, doi: 10.1093/mnras/staa3150

Mirocha, J., & Furlanetto, S. R. 2023, MNRAS, 519, 843, doi: 10.1093/mnras/stac3578

Morales, A. M., Finkelstein, S. L., Leung, G. C. K., et al. 2024, ApJL, 964, L24, doi: 10.3847/2041-8213/ad2de4

Morishita, T., Stiavelli, M., Chary, R.-R., et al. 2024, ApJ, 963, 9, doi: 10.3847/1538-4357/ad1404

Muñoz, J. B., Mirocha, J., Chisholm, J., Furlanetto, S. R., & Mason, C. 2024, arXiv e-prints, arXiv:2404.07250, doi: 10.48550/arXiv.2404.07250

Muñoz, J. B., Mirocha, J., Furlanetto, S., & Sabti, N. 2023, MNRAS, 526, L47, doi: 10.1093/mnrasl/slad115

Murray, S. G., Power, C., & Robotham, A. S. G. 2013, Astronomy and Computing, 3, 23, doi: 10.1016/j.ascom.2013.11.001

Naidu, R. P., Matthee, J., Oesch, P. A., et al. 2022, MNRAS, 510, 4582, doi: 10.1093/mnras/stab3601

Nakane, M., Ouchi, M., Nakajima, K., et al. 2023, arXiv e-prints, arXiv:2312.06804, doi: 10.48550/arXiv.2312.06804

Narayanan, D., Lower, S., Torrey, P., et al. 2024, ApJ, 961, 73, doi: 10.3847/1538-4357/ad0966

Ouchi, M., Shimasaku, K., Furusawa, H., et al. 2010, ApJ, 723, 869, doi: 10.1088/0004-637X/723/1/869

Paardekooper, J.-P., Khochfar, S., & Dalla Vecchia, C. 2015, MNRAS, 451, 2544, doi: 10.1093/mnras/stv1114

Pahl, A. J., Shapley, A., Steidel, C. C., Reddy, N. A., & Chen, Y. 2022, MNRAS, 516, 2062, doi: 10.1093/mnras/stac1767

Pahl, A. J., Shapley, A., Steidel, C. C., et al. 2023, MNRAS, 521, 3247, doi: 10.1093/mnras/stad774

Pallottini, A., & Ferrara, A. 2023, A&A, 677, L4, doi: 10.1051/0004-6361/202347384

Pallottini, A., Ferrara, A., Gallerani, S., et al. 2022, MNRAS, 513, 5621, doi: 10.1093/mnras/stac1281

Pérez-González, P. G., Costantin, L., Langeroodi, D., et al. 2023, ApJL, 951, L1, doi: 10.3847/2041-8213/acd9d0

Planck Collaboration, Aghanim, N., Akrami, Y., et al. 2020, A&A, 641, A6, doi: 10.1051/0004-6361/201833910

Prieto-Lyon, G., Strait, V., Mason, C. A., et al. 2023, A&A, 672, A186, doi: 10.1051/0004-6361/202245532

Qin, Y., Mesinger, A., Bosman, S. E. I., & Viel, M. 2021, MNRAS, 506, 2390, doi: 10.1093/mnras/stab1833

Qiu, Y., Wyithe, J. S. B., Oesch, P. A., et al. 2018, MNRAS, 481, 4885, doi: 10.1093/mnras/sty2633

Rasmussen Cueto, E., Hutter, A., Dayal, P., et al. 2023, arXiv e-prints, arXiv:2312.12109, doi: 10.48550/arXiv.2312.12109

Reed, D. S., Bower, R., Frenk, C. S., Jenkins, A., & Theuns, T. 2007, MNRAS, 374, 2, doi: 10.1111/j.1365-2966.2006.11204.x

Ren, K., Trenti, M., & Mason, C. A. 2019, ApJ, 878, 114, doi: 10.3847/1538-4357/ab2117

Senchyna, P., Plat, A., Stark, D. P., & Rudie, G. C. 2023, arXiv e-prints, arXiv:2303.04179, doi: 10.48550/arXiv.2303.04179

Shen, X., Vogelsberger, M., Boylan-Kolchin, M., Tacchella, S., & Kannan, R. 2023, MNRAS, 525, 3254, doi: 10.1093/mnras/stad2508

Sheth, R. K., Mo, H. J., & Tormen, G. 2001, MNRAS, 323, 1, doi: 10.1046/j.1365-8711.2001.04006.x

Sobacchi, E., & Mesinger, A. 2015, MNRAS, 453, 1843, doi: 10.1093/mnras/stv1751

Sparre, M., Hayward, C. C., Feldmann, R., et al. 2017, MNRAS, 466, 88, doi: 10.1093/mnras/stw3011

Stark, D. P., Schenker, M. A., Ellis, R., et al. 2013, ApJ, 763, 129, doi: 10.1088/0004-637X/763/2/129

Steidel, C. C., Bogosavljević, M., Shapley, A. E., et al. 2018, ApJ, 869, 123, doi: 10.3847/1538-4357/aaed28

Strait, V., Brammer, G., Muzzin, A., et al. 2023, ApJL, 949, L23, doi: 10.3847/2041-8213/acd457

Sun, G., Faucher-Giguère, C.-A., Hayward, C. C., & Shen, X. 2023a, MNRAS, 526, 2665, doi: 10.1093/mnras/stad2902

Sun, G., Faucher-Giguère, C.-A., Hayward, C. C., et al. 2023b, ApJL, 955, L35, doi: 10.3847/2041-8213/acf85a

Tacchella, S., Bose, S., Conroy, C., Eisenstein, D. J., & Johnson, B. D. 2018, ApJ, 868, 92, doi: 10.3847/1538-4357/aae8e0

Tang, M., Stark, D. P., Chevallard, J., & Charlot, S. 2019, MNRAS, 489, 2572, doi: 10.1093/mnras/stz2236

Tang, M., Stark, D. P., Chevallard, J., et al. 2021, MNRAS, 503, 4105, doi: 10.1093/mnras/stab705

Tinker, J. L., Robertson, B. E., Kravtsov, A. V., et al. 2010, ApJ, 724, 878, doi: 10.1088/0004-637X/724/2/878

Topping, M. W., Stark, D. P., Endsley, R., et al. 2024a, MNRAS, 529, 4087, doi: 10.1093/mnras/stae800

Topping, M. W., Stark, D. P., Senchyna, P., et al. 2024b, MNRAS, 529, 3301, doi: 10.1093/mnras/stae682

Trinca, A., Schneider, R., Valiante, R., et al. 2024, MNRAS, 529, 3563, doi: 10.1093/mnras/stae651

Trussler, J., Conselice, C., Adams, N., et al. 2024, arXiv e-prints, arXiv:2404.07163, doi: 10.48550/arXiv.2404.07163

Umeda, H., Ouchi, M., Nakajima, K., et al. 2023, arXiv e-prints, arXiv:2306.00487, doi: 10.48550/arXiv.2306.00487

Wechsler, R. H., & Tinker, J. L. 2018, ARA&A, 56, 435, doi: 10.1146/annurev-astro-081817-051756

Weisz, D. R., Johnson, B. D., Johnson, L. C., et al. 2012, ApJ, 744, 44, doi: 10.1088/0004-637X/744/1/44

Whitler, L., Stark, D. P., Endsley, R., et al. 2023, MNRAS, 519, 5859, doi: 10.1093/mnras/stad004

Whitler, L. R., Mason, C. A., Ren, K., et al. 2020, MNRAS, 495, 3602, doi: 10.1093/mnras/staa1178

Zackrisson, E., Inoue, A. K., & Jensen, H. 2013, ApJ, 777, 39, doi: 10.1088/0004-637X/777/1/39